Local Self-Consistent Ornstein−Zernike Integral Equation Theory and Application to a Generalized Lennard-Jones Potential

Shiqi Zhou*

School of Physics Science and Technology, Central South University, Changsha, Hunan 410083, China
State Key Laboratory of Powder Metallurgy, Central South University, Changsha, Hunan 410083, China

Received: April 28, 2010; Revised Manuscript Received: July 23, 2010

Local self-consistent Ornstein−Zernike (OZ) integral equation theory (IET) provides a rapid and easy route for obtaining independently thermodynamic and structural information for a single state point. Because of neglect of information of neighboring state points in determining a self-consistent adjustable parameter performance of the local self-consistent OZ IET is somewhat vulnerable and worthy of intensive investigation. For this reason, we have performed Monte Carlo simulations to obtain thermodynamic and structural properties of fluid with a generalized Lennard-Jones potential, and the present simulation results are employed to verify the quality of a local version of a recently developed global self-consistent OZ IET and a local expression for computation of excess chemical potential directly from the structural functions of the state point of interest. Comprehensive comparison and analysis demonstrate the following (i) the present local self-consistent OZ IET performs quite well for calculation of pressure and excess internal energy; (ii) using the same structural functions from the present local self-consistent OZ IET, the previously derived local expression by the present author has by and large the same accuracy in calculating the excess chemical potential as an exact virial formula for the pressure; (iii) although the excellent performance exhibited for the above thermodynamic quantities persists to very low temperature and very short-ranged potential and remains even in the liquid−solid coexistence region, the excess Helmholtz free energy calculated from the pressure and excess chemical potential shows evident inaccuracy for a density−temperature combination deep in the liquid−solid coexistence region, and this makes it necessary to derive a local formulation for the excess free energy.

I. Introduction

Intermolecular interactions are rudimentary input information for condensed matter studies. One of the fundamental objectives of classical statistical mechanics[1] is to predict microscopic structural information and macroscopic thermodynamic properties from the intermolecular interactions dominating the micromovement of the particles comprising the thermodynamic system under consideration. The intermolecular interactions[2] originate from electromagnetic forces between the electrons and the nuclei forming the molecules; because of the quantum-mechanical character of the motion of these particles, a rigorous theory of intermolecular forces requires a solution of the Schrödinger equation for a system of interacting molecules. Although advances in computational techniques, particularly ab initio calculations, have made it possible to describe the intermolecular interactions in considerable detail, use of models of intermolecular potentials retains its importance for a vast number of applications[3] mainly because of increase of the computational effort in proportion to a high power of the number of electrons which makes the application of the former approach to molecules containing more than a few atoms impracticable.

The intermolecular interactions are usually represented in terms of pair potentials that are to be regarded as effective potentials taking into account, in some average sense, the contribution of many-body effects. An essential feature of the interatomic interaction is a highly steep repulsion at short interparticle separation caused by an overlap of outer electron shells and a van der Waals interaction which is caused by a change in dipole moment arising from a shift of orbital electrons to one side of an atom or molecule, creating a similar shift in adjacent atoms or molecules. These van der Waals forces are always present between molecules or between particles, and may be attractive or repulsive.[4] For like materials, the van der Waals forces are always attractive; however, repulsive forces are predicted for certain dissimilar material combinations. The well-known Lennard-Jones (LJ) potential incorporates the two behaviors into a single potential function having the form

$$u(r) = 4\varepsilon\left[\left(\frac{\sigma}{r}\right)^{12} - \left(\frac{\sigma}{r}\right)^{6}\right] \quad (1)$$

In eq 1, ε is the depth of the potential minimum called the energy parameter and σ, a so-called size parameter, is the separation at which the potential energy disappears. The LJ potential yields a phase diagram reproducing the behavior of typical monatomic substances featured by a vapor−liquid critical point and a vapor−liquid−solid triple point; as a result, the LJ potential is believed to provide an adequate description of the interactions being in operation between pairs of rare gas atoms and other approximately spherical molecules such as CH_4. The energy and size parameter ε and σ are determined by fitting measured physical properties, such as the second virial coefficient.

The van der Waals forces also contribute to an understanding of the liquid behavior of complex macromolecules; one example is the interactions of proteins with other molecules or with surfaces. Forces dominating the interaction of protein molecules with like proteins, with different proteins, and with other materials include electrostatic forces, van der Waals forces,

* E-mail: chixiayzsq@yahoo.com.

10.1021/jp1038317
Published on Web 08/12/2010

solvation forces, etc. It is noted[5] that all of these forces play important roles in the context of molecular recognition processes, dynamics of aggregation, precipitation, crystal growth, colloidal stability, etc. One main difference between the van der Waals forces occurring in the two contexts is different potential ranges. Because of the relatively large particle size, the van der Waals forces working in the context of macromolecules are short-ranged,[5g] and consequently, the standard LJ potential is too long-ranged, and not qualified for helping in describing the thermodynamic and structural properties of the macromolecules in solution. A generalized LJ potential is given by

$$u(r) = 4\varepsilon\left[\left(\frac{\sigma}{r}\right)^{2n} - \left(\frac{\sigma}{r}\right)^{n}\right] \tag{2}$$

This is a simple one-parameter model (henceforth also referred to as the GLJ $2n - n$ potential) for tuning the interaction range and serves well for modeling of the van der Waals forces playing a role in building macromolecular force fields by increasing the value of the exponent n and making the potential short-ranged; one of the examples is the well-known DLVO theory,[5g] in which an attractive van der Waals term, which is short-ranged on the scale of colloid diameter and thus somewhat similar to the attractive term of the GLJ $2n - n$ potential with n being attached by a high value, accounts for the stability issue of the charged colloids by combining with a Debye−Hückel-like electrostatic contribution. Phase diagrams of this system were calculated, respectively, by using a density functional approach[6] and a computer simulation technique,[7] and it is found that the two routes lead to reasonably consistent results. The simulations are focused on four values of n, namely, $n = 6$ which is long-ranged and the classical model for simple liquids, $n = 11$ and $n = 12$ which are medium- to short-ranged, and $n = 18$ which is very short-ranged.

One notes that an Ornstein−Zernike (OZ) integral equation theory (IET)[8a] had been successfully applied to a range of isotropic and homogeneous fluids, and played a key role in predicting thermodynamic functions and structural functions of bulk liquids, particularly colloidal fluids,[8b−f] from the intermolecular interactions. However, to our knowledge, systematic work has not been reported for an applicability of the OZ IET to the GLJ $2n - n$ potential. The OZ IET is defined by an OZ IE and an approximation for a bridge function needed to close the OZ IE which refers to two structural functions. It is realized that early successful approximations (see ref 9 and references therein) such as the Percus−Yevick (PY) approximation, hypernetted chain (HNC) approximation, mean spherical approximation (MSA), and so on, produce predictions deviating evidently from the "exact" computer simulation results. Subsequent revisions[10] on these early approximations are characterized by one or several adjustable parameter(s) which is used to force an equality of thermodynamic quantities obtained from different routes based on the same numerically solved structural functions information, and such closures and the resulting OZ ITE approaches are called the self-consistent OZ IET approach; some of the relevant examples can be listed.[10−13] It is the different procedure used to determine the adjustable parameter(s) which makes a distinction between local and global procedures. The global procedure determines the adjustable parameter(s) by solving the OZ IET over a wide domain in the phase diagram, and from the current experience, it is noted that the global procedure is relatively more accurate than the local procedure, but the price to pay is that one has to solve numerically the OZ IE at many state points even if one only needs information for one single state point; the price to pay also includes the complexity of programming which manifests itself clearly when the vapor−liquid two phase region has to be skirted around. In contrast, the local procedure is far less computationally intensive than the global procedure, as it only needs to solve numerically the OZ IE at two state points to determine the adjustable parameter(s) for one state point of interest; consequently, the local procedure can be applied with equal ease to both supercritical and subcritical regions of the phase diagram. The only undesirable point relevant to the local procedure is that the performance may decline somewhat, as the local procedure ignores the dependence of the adjustable parameter(s) on a density argument. In the present paper, "local procedure" additionally includes another meaning, namely, a local formulation[12,18] for obtaining an excess chemical potential from structural functions without a thermodynamic integration. Since pressure can be calculated by a virial route locally, once the excess chemical potential is obtained locally, all of the thermodynamic properties can be obtainable locally; the self-consistent OZ IET approach advanced in ref 12 is local according to the mentioned double standards. One easily understands that the self-consistent OZ IET approach critically depends on the approximation employed for the bridge function. Recently, a bridge function approximation was proposed,[13] and the resulting global self-consistent OZ IET approach is employed to calculate for an imaginary fluid a radial distribution function (rdf) and an excess Helmholtz free energy both of which are used as input to switch on a recently proposed non-hard-sphere thermodynamic perturbation theory.[13] The aim of the present paper is twofold. First, the recent bridge function approximation[13] is combined with the local procedure[12] to formulate a local self-consistent OZ IET approach which will then be applied to the GLJ $2n - n$ potential for confirmation of its validity; second, extensive Monte Carlo simulation is carried out to provide rdf and thermodynamic functions of the GLJ $2n - n$ potential for supporting the mentioned validation process, and simulated data for a static structure factor of the GLJ $2n - n$ potential supplied in ref 7 are borrowed to compare with the present local self-consistent OZ IET results.

The layout of the present paper is as follows. Details of the present local self-consistent OZ IET and simulation technique are briefly described in section II, which is followed by a presentation and discussion of the simulation and theory's results in section III. Finally, our conclusions are drawn in section IV.

II. Theory and Simulation

II.1. Local Self-Consistent OZ IET Approach. For a single component fluid with a center symmetrical potential like eq 2, the OZ IET is defined by an OZ IE together with a closure equation involving an unknown bridge function $B(r)$. The OZ IE takes the form

$$h(r) = c(r) + \rho \int \mathrm{d}\mathbf{r}' h(\mathbf{r}') c(|\mathbf{r} - \mathbf{r}'|) \tag{3}$$

The closure equation is described as

$$h(r) + 1 = \exp\{-\beta u(r) + \gamma(r) + B(r)\} \tag{4}$$

where $h(r) = g(r) - 1$ and $\gamma(r) = h(r) - c(r)$ are total and indirect correlation functions, respectively; $g(r)$ and $c(r)$ are, respectively, the rdf and direct correlation function (DCF); and ρ is the number density of the fluid under consideration. $B(r)$ is

the so-called bridge function which consists of an infinite series of highly connected diagrams and refers to special multidimensional integrals.

One of the aims of the present paper is to test a local self-consistent OZ IET in which we will, by closely following the procedure of ref 12, use a recent hard sphere bridge function[13] to approximate the bridge function of interest and adjust the hard sphere diameter entering the hard sphere bridge function[13] to deviate from the size parameter σ of the potential function of interest to enforce a local consistency condition; i.e., the reduced isothermal compressibility from the virial route and the fluctuation route should be equal. Details of the present local self-consistent OZ IET are summarized as follows.

The hard sphere bridge function[13] is a hybrid of a Malijevsky−Labik hard sphere bridge function denoted by subscript ML[14] for the domain of $r > \sigma_{HS}$ and a recently proposed GvEF−BS−VW hard sphere bridge function due to the present author[12] for the domain of $r < \sigma_{HS}$. To make the hybrid hard sphere bridge function continuous at $r = \sigma_{HS}$, the GvEF−BS−VW hard sphere bridge function for $r < \sigma_{HS}$ should be shifted a density-dependent constant; the hybrid hard sphere bridge function[13] is given by

$$B_{HS}(r/\sigma_{HS}, \rho_{HS}\sigma_{HS}^3) = \begin{cases} B_{ML}(r/\sigma_{HS}, \rho_{HS}\sigma_{HS}^3) & r > \sigma_{HS} \\ B_{GvEF-BS-VW}(r/\sigma_{HS}, \rho_{HS}\sigma_{HS}^3) + \text{Cons} & r < \sigma_{HS} \end{cases} \quad (5)$$

where $\text{Cons} = B_{ML}(1, \rho_{HS}\sigma_{HS}^3) - B_{GvEF-BS-VW}(1, \rho_{HS}\sigma_{HS}^3)$ and σ_{HS} and ρ_{HS} are, respectively, the hard sphere diameter and number density. Details of the GvEF−BS−VW hard sphere bridge function are documented in an appendix to the paper.

Following refs 12 and 13, $B(r)$ of the present interest can be approximated by the above hard sphere bridge function with σ_{HS} and ρ_{HS} being substituted by an effective hard sphere diameter d_{eff} and ρ, namely,

$$B(r/\sigma, \rho\sigma^3) = B_{HS}(r/d_{eff}, \rho d_{eff}^3) \quad (6)$$

The local consistency condition for specification of d_{eff} takes the following form:

$$\frac{\chi_0}{\chi_T^v} = \frac{\chi_0}{\chi_T^c} \quad (7)$$

The virial reduced isothermal compressibility χ_0/χ_T^v is calculated by a finite difference method

$$\frac{\chi_0}{\chi_T^v} = \beta\frac{\partial P^v}{\partial \rho} = \frac{\beta P^v(\rho^* + \mathrm{d}\rho^*, T^*, d_e) - \beta P^v(\rho^*, T^*, d_e)}{\mathrm{d}\rho} \quad (8)$$

the virial pressure P^v is calculated from the virial route

$$\frac{\beta P^v}{\rho} = 1 - \frac{\beta\rho}{6}\int_0^\infty \mathrm{d}r 4\pi r^3 \frac{\mathrm{d}u(r)}{\mathrm{d}r} g(r) \quad (9)$$

whereas the reduced isothermal compressibility χ_0/χ_T^c throughout the fluctuation route reads

$$\frac{\chi_0}{\chi_T^c} = \beta\frac{\partial P^c}{\partial \rho} = 1 - \rho\int \mathrm{d}\mathbf{r} c(r; \rho) \quad (10)$$

Throughout the paper, the reduced density ρ^* is defined as $\rho\sigma^3$, the reduced temperature T^* is defined by k_BT/ε where k_B is the Boltzmann constant and T is the absolute temperature, $\beta = 1/k_BT$, and $|\mathrm{d}\rho^*|$ is a conveniently small density increment (typically 10^{-4}). For the case of supercritical state, $\mathrm{d}\rho^*$ can be positive or negative, whereas, for the case of subcritical state, $\mathrm{d}\rho^*$ is usually chosen as positive when the state point is adjacent to the liquid phase side of the vapor−liquid coexistence curve and negative when the state point is adjacent to the vapor phase side of the vapor−liquid coexistence curve. Throughout the text, according to convenience, we will use reduced quantities or conventional quantities. As the procedure for determining the adjustable parameter d_{eff} only refers to the most neighboring state point, we designate the procedure as a "local" procedure. The local procedure is characterized ignoring the dependence of d_{eff} on the involved density argument by using the same value of d_{eff} to calculate the virial pressures of two neighboring state points with different densities (see eq 8).

Once the OZ IET is solved, the static structure factor $S(k)$ is readily computable from the resulting $c(r)$:

$$S(k) = 1/(1 - \rho\hat{c}(k)) \quad (11)$$

The excess internal energy per particle u_{ex} is directly obtainable from the rdf $g(r)$:

$$u_{ex} = 2\pi\rho\int u(r)g(r)r^2\,\mathrm{d}r \quad (12)$$

Next, we will discuss local computation of an excess chemical potential μ_{ex} from structural functions acquired by the local self-consistent OZ IET. Traditional methods include a Gibbs−Duhem (GD) relation that is concerned with a thermodynamic integration along an isothermal path and a classical formula of Kirkwood[15] which refers to, for aim of integration, numerous calculations of the pair correlation functions with different values of a charging parameter. These two approaches are therefore designated as "global". Recently, the present author proposed[12] a "local" formulation which makes the excess chemical potential obtainable directly from the structural functions of the state point of interest:

$$\beta\mu_{ex} = \rho\int_0^\infty \Big(\gamma(r) - h(r) + \alpha(\rho^*, T^*)B(r) + \frac{1}{2}h(r)(\gamma(r) + \alpha(\rho^*, T^*)B(r))\Big)4\pi r^2\,\mathrm{d}r \quad (13)$$

Upon acquirement of the structural functions, the scaling parameter $\alpha(\rho^*, T^*)$ is determined by a sum rule

$$\beta\frac{\partial\mu_{ex}}{\partial\rho}\bigg|_{T^*} = -4\pi\int \mathrm{d}r r^2 c(r) \quad (14)$$

The derivative associated with eq 14 is obtainable by the finite difference method and ignoring the density dependence of the scaling parameter $\alpha(\rho^*, T^*)$

$$\beta\frac{\partial\mu_{ex}}{\partial\rho}\bigg|_{T^*} = \frac{\beta\mu_{ex}(\rho^* + \Delta\rho^*, T^*, \alpha(\rho^*, T^*)) - \beta\mu_{ex}(\rho^*, T^*, \alpha(\rho^*, T^*))}{\Delta\rho} \quad (15)$$

where $\Delta\rho^*$ is a small density increment whose choice is similar to that of the foregoing $d\rho^*$.

Once the virial pressure p^v and the excess chemical potential μ_{ex} are available, the excess Helmholtz free energy per particle f_{ex} divided by kT can be obtainable by a basic thermodynamic relationship:

$$\beta f_{ex} = \beta\mu_{ex} - \frac{\beta p^v}{\rho} + 1 \quad (16)$$

II.2. *NVT*-Monte Carlo Simulation. The constant *NVT*-Monte Carlo simulation[16] is employed to obtain the rdf $g(r)$, pressure p, and excess internal energy per particle u_{ex}. The simulations are performed in a cubic cell subject to periodic boundary conditions. The simulated system consists of $N = 500$ particles initially placed in a low-density fcc configuration, and the box length is adjusted so that the number density in the cubic cell is exactly equal to the number density of interest. Then, the system was equilibrated at the desired reduced temperature T^* for $N_e = 6 \times 10^4$ cycles; each cycle consists of 500 attempted moves over a randomly selected particle, and the acceptance ratio was fixed at around 50% by adjusting the maximum displacement. The thermodynamic properties were determined from averages performed over the next $N_s = 1.5 \times 10^5$ cycles. p and u_{ex} are sampled every 500 cycles, from which the statistical uncertainty is estimated as the standard deviation. The pressure p is directly obtainable in simulation by the virial route:

$$p = \rho kT\left(1 - \frac{1}{3N}\left\langle\sum_i\sum_{j>i} r_{ij}\frac{\partial\beta u(r_{ij})}{\partial r_{ij}}\right\rangle\right) \quad (17)$$

For the GLJ $2n - n$ potential with high values of exponent n, the repulsive part is very steep, an accurate computation of the virial pressure is difficult in simulations, and a considerable number of cycles, as employed in the present study, are needed in order to obtain satisfactory accuracy of the pressure p. u_{ex}, actually a thermal average of the interaction potential energy, is directly obtainable in simulation

$$u_{ex} = \frac{1}{N}\langle\sum_i\sum_{j>i} u(r_{ij})\rangle \quad (18)$$

For the supercritical state, $\beta f_{ex}(\rho^*, T^*)$ can be calculated by integrating along an isothermal line:

$$\beta f_{ex}(\rho^*, T^*) = \int_0^{\rho^*}\frac{(Z(\rho'^*, T^*) - 1)}{\rho'^*}\,d\rho'^* \quad (19)$$

here, $Z(\rho^*, T^*) = p^*/\rho^*T^*$ is the compressibility factor with reduced pressure p^* being defined as $p\sigma^3/\varepsilon$. For the subcritical state, $\beta f_{ex}(\rho^*, T^*)$ can be obtained by integrating along an isochore:

$$\beta f_{ex}(\rho^*, T^*) = \beta f_{ex}(\rho^*, T_0^*) + \int_{1/T_0^*}^{1/T^*} u_{ex}^*(\rho^*, T'^*)\,d(1/T'^*) \quad (20)$$

here, $u_{ex}^*(\rho^*, T^*) = u_{ex}(\rho^*, T^*)/\varepsilon$ is the reduced excess internal energy; T_0^* is usually chosen to be a suitably high temperature, for example, $T_0^* = 5$ as done in the present paper. It is noted that, for state points characterized with such high T_0^*, the Widom test particle insertion method is very efficient for simulation of the excess chemical potential $\beta\mu_{ex}(\rho^*, T_0^*)$ whether the density ρ^* is high or low. Once $\beta\mu_{ex}(\rho^*, T_0^*)$ is acquired by the Widom test particle insertion method and $Z(\rho^*, T_0^*)$ is obtained by the virial route, $\beta f_{ex}(\rho^*, T_0^*)$ will be obtainable by the basic thermodynamic relationship in eq 16. To obtain $\beta\mu_{ex}(\rho^*, T_0^*)$ with $T_0^* = 5$ in the *NVT*-Monte Carlo simulation, it is sufficiently safe to take $N_e = 6 \times 10^4$ and $N_s = 1.5 \times 10^5$ with 10^6 trial insertions during each sampling every 500 cycles. In all simulations, the interaction potential is truncated at $r_c \leq$ half simulation box length but not shifted and the excess internal enery, pressure, and excess chemical potential are corrected with tail contributions in a mean field approximation.[16]

III. Results and Discussion

The vapor−liquid and liquid−solid coexistence curves for the GLJ $2n - n$ potential with varying n were calculated by computer simulation[7] and theory;[6] these phase diagrams are useful for the discussion presented below. We will first discuss the structural functions, and a comparison between simulation results and present theoretical results is displayed in Figures 1 and 2 for the rdf and in Figure 3 for the static structure factor. The rdf is calculated for state points featured by near triple point (Figure 1a), near critical point (Figure 1b,c) and sinking in the liquid−solid coexistence region (Figures 1c and 2). Two observations can be confirmed from these calculations. (i) The two routes agree with each other very satisfactorily except for those state points (Figures 1c and 2) situated within the liquid−solid coexistence region. (ii) When the calculated state points sink in the liquid−solid coexistence region, as displayed in Figures 1c and 2, an unusual peak is ready to come out between the first and second normal peaks in the fluid rdf curve. Deeper and deeper into the liquid−solid coexistence region, the additional unusual peak becomes more pronounced, and this seems to indicate that the system is a fluid with embedded quasi-crystalline clusters. Like other liquid state theories, the present local self-consistent OZ IET is also incapable of describing the emergence of the peak characterizing the quasi-crystalline structures; however, global morphology of the rdf is still delineated accurately. It should be pointed out that, to simulate the liquid phase configuration of state points situated within the liquid−solid coexistence region, an equilibrium configuration of the state point situated in a single liquid phase region should be used as the initial configuration of the simulated system.

Figure 3 presents a comparison between simulation results available in the literature[7] and present theoretical results for the static structure factor; the calculated state points are, respectively, near the triple point (Figure 3a) and near the liquid side of the liquid−solid coexistence curve (Figure 3b and c). It is noted that for these "dangerous" states the reported simulation data is rather scattered; generally speaking, the present theoretical calculation satisfactorily describes the trend of $S(k)$ versus k curve. For these three state points, particularly the state point displayed in Figure 3b which is also very adjacent to the critical point, density fluctuations are evident, and this can be seen from the upswing in $S(k)$ at low $k\sigma$; encouragingly, the present local

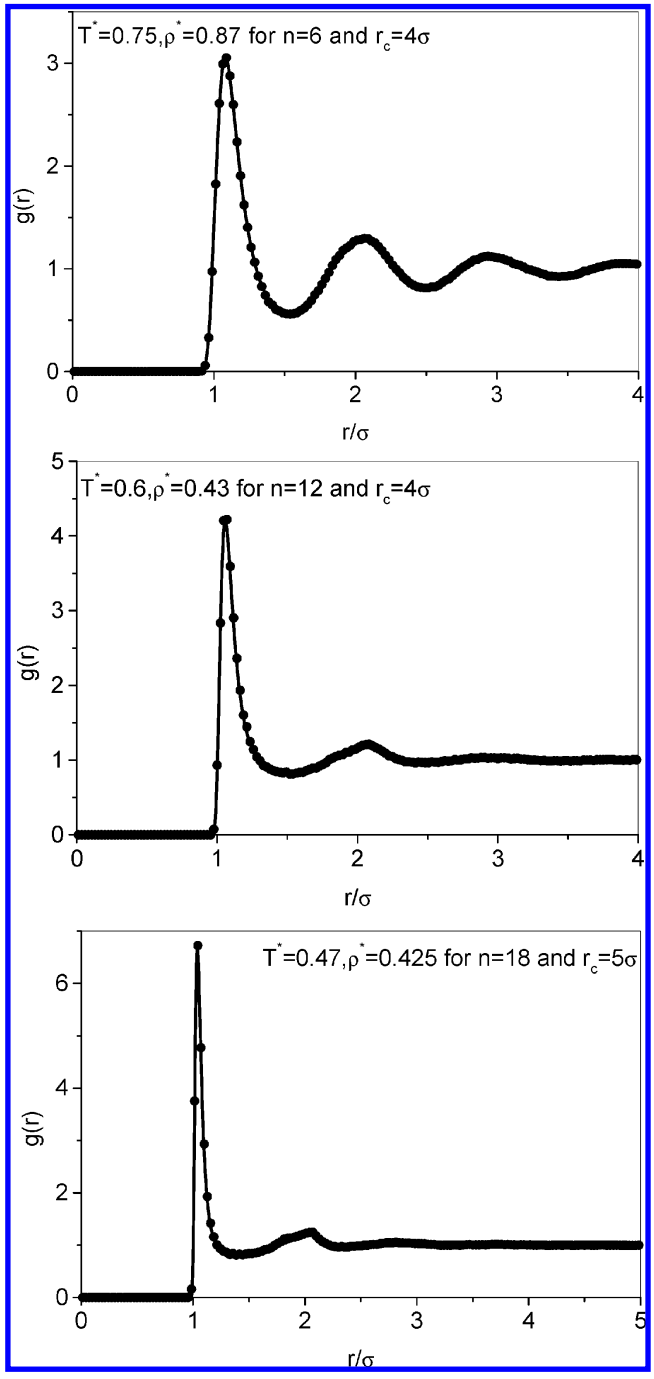

Figure 1. Radial distribution function $g(r)$ for the GLJ $2n - n$ fluid with varying values of exponent n as shown together with other bulk parameters. Circles represent the present computer simulation data, whereas lines are for the present theoretical calculation results. The simulations are for the GLJ $2n - n$ fluid potential truncated at r_c but not shifted; correspondingly, the local self-consistent OZ IET calculations are also for the same system truncated at r_c but not shifted.

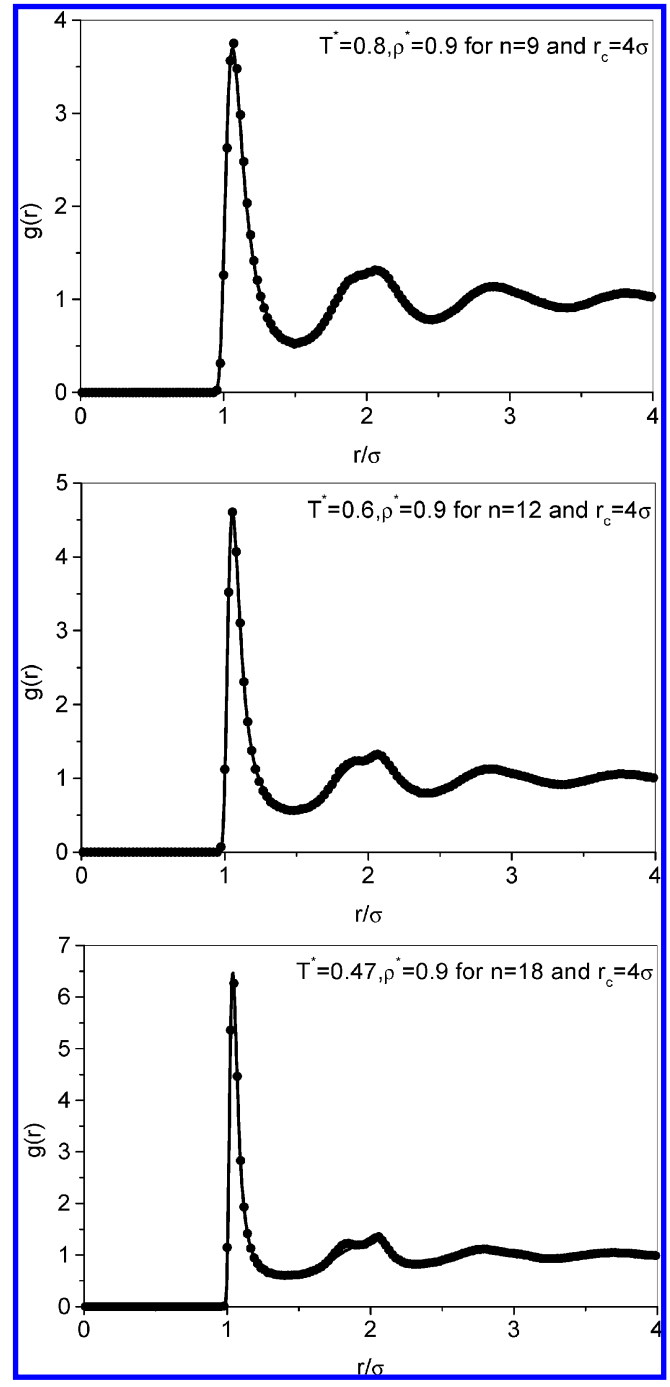

Figure 2. Same as in Figure 1 but for different bulk parameters as shown.

self-consistent OZ IET very satisfactorily describes these characteristics.

Figures 4−7 exhibit the trend of four thermodynamic properties along an isochore for the GLJ $2n - n$ potential with $n = 6$ and density $\rho^* = 0.85$; the range of the calculated temperature extends to be close to the triple point temperature. Both p^* and u_{ex}^* are obtained directly in simulation by eqs 17 and 18, whereas f_{ex}/k_BT is obtained by integrating along an isochore and μ_{ex}/k_BT is calculated by the basic thermodynamic relationship in eq 16. The integral calculation in eq 20 needs as input T_0^* and $\beta f_{ex}(\rho^*, T_0^*)$; to achieve this goal, we choose $T_0^* = 5$ and carry out the *NVT*-MC simulation using the Widom test particle insertion method to obtain $\mu_{ex}/k_BT = 4.779$ and $p^* = 18.35864$ for the state point characterized with $T_0^* = 5$ and $\rho^* = 0.85$; this leads to the needed information of $\beta f_{ex} = 1.45932$. From Figures 4−7, one observes that, for this relatively long-ranged potential, the local self-consistent OZ IET accurately predicts the pressure, excess internal energy, and excess chemical potential; comparatively speaking, the excess free energy is less accurate. It is noted that the excess free energy is calculated by eq 16 which needs as input information the pressure and excess chemical potential; since the two input quantities are themselves approximate, the resulting excess free energy is inevitably involved with double approximations, and this explains why the theoretical excess free energy calculated in this way is less satisfactory.

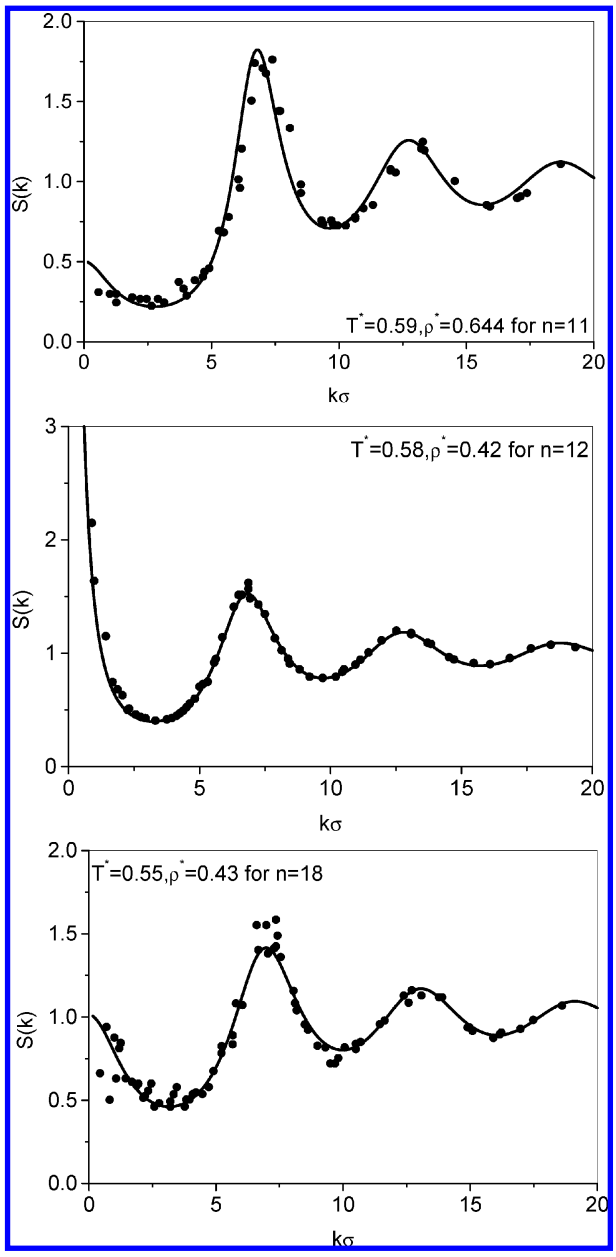

Figure 3. Same as in Figure 1 except that the calculations are for the static structure factor $S(k)$ and different bulk parameters as shown. The simulation data are borrowed from ref 7, and the potential is not truncated.

Figures 8−11 display the four thermodynamic quantities as a function of density for the GLJ $2n - n$ potential with $n = 12$; the temperatures are fixed at several different values. Similar to Figures 4−7, p^* and u_{ex}^* are calculated directly in simulation by eqs 17 and 18, whereas f_{ex}/k_BT is obtained by integrating along an isotherm denoted by eq 19, and μ_{ex}/k_BT is calculated by the basic thermodynamic relationship eq 16. To constitute a rigorous test, the density range extends into the solid−liquid coexistence region and the temperature is chosen to be adjacent to the critical temperature. Figures 12−15 present results similar to those in Figures 8−11 except that the calculations are for the GLJ $2n - n$ potential with $n = 18$, and the temperature is chosen to be adjacent to the critical temperature for the GLJ $2n - n$ potential with $n = 18$. It is noted that an observation similar to that just discussed for Figures 4−7 can be drawn from Figures 8−15; i.e., the pressure, excess internal energy, and excess chemical potential are more accurately predicted than the excess

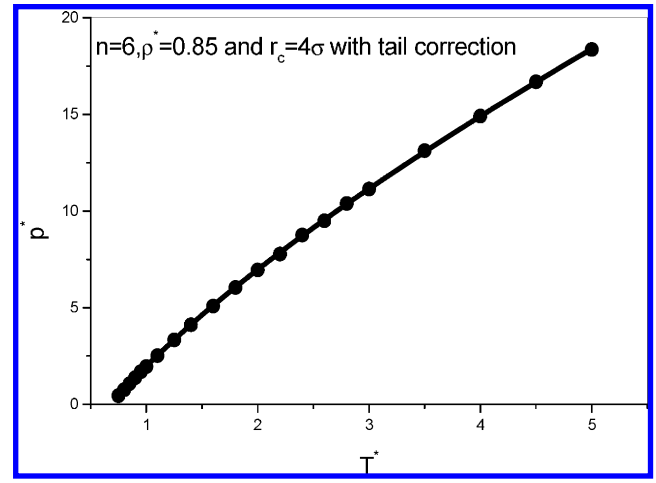

Figure 4. The reduced pressure p^* along with an isochore. The calculations are for the GLJ $2n - n$ fluid with $n = 6$ and $\rho^* = 0.85$; the potential is truncated at $r_c = 4\sigma$ but not shifted, and the simulated pressures are corrected with tail contributions in a mean field approximation. Circles represent the present computer simulation data, whereas lines are for the present theoretical calculation results for the full potential.

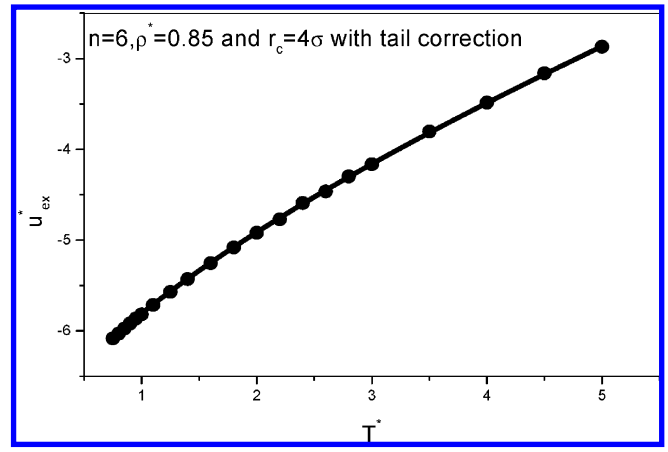

Figure 5. Same as in Figure 4, but the results are for the reduced excess internal energy u_{ex}^*.

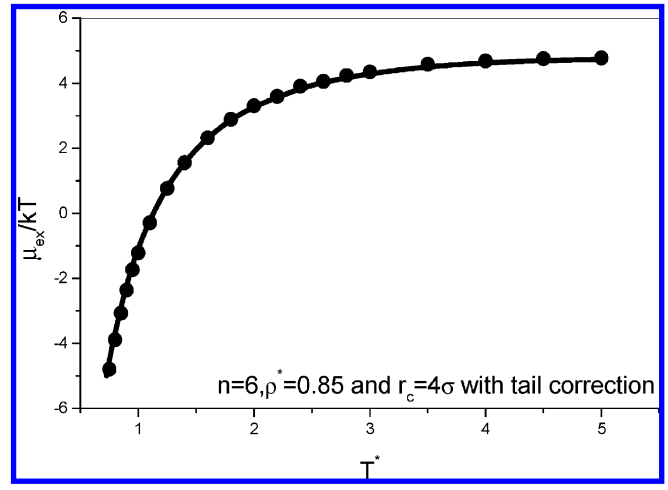

Figure 6. Same as in Figure 4, but the results are for the reduced excess chemical potential μ_{ex}/k_BT.

free energy. Several new observations are listed as follows. (i) With shortening of the potential range, the overall accuracy of the local self-consistent OZ IET declines somewhat for all calculated quantities, this is in accordance with all previous

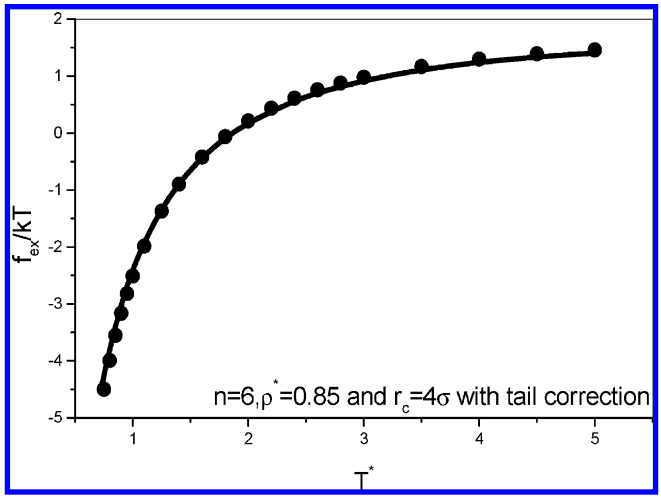

Figure 7. Same as in Figure 4 but the results are for the reduced excess free energy f_{ex}/k_BT.

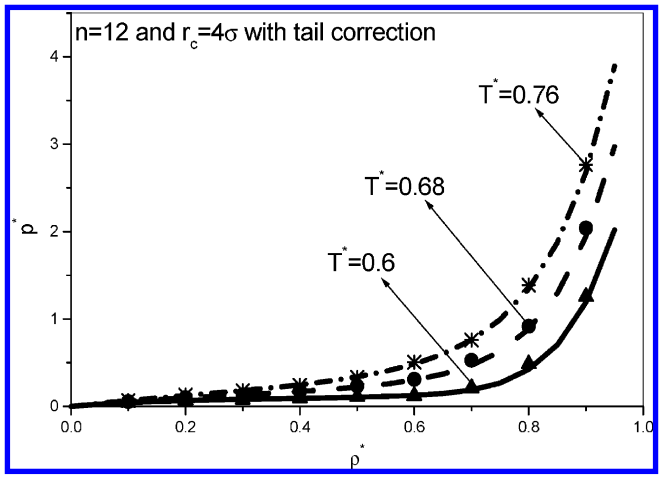

Figure 8. The reduced pressure p^* along with an isothermal line. The calculations are for the GLJ $2n - n$ fluid with $n = 12$ and several different temperature values as shown; the potential is truncated at $r_c = 4\sigma$ but not shifted, the simulated pressure are corrected with tail contributions in a mean field approximation. Circles represent the present computer simulation data, whereas lines are for the present theoretical calculation results for the full potential.

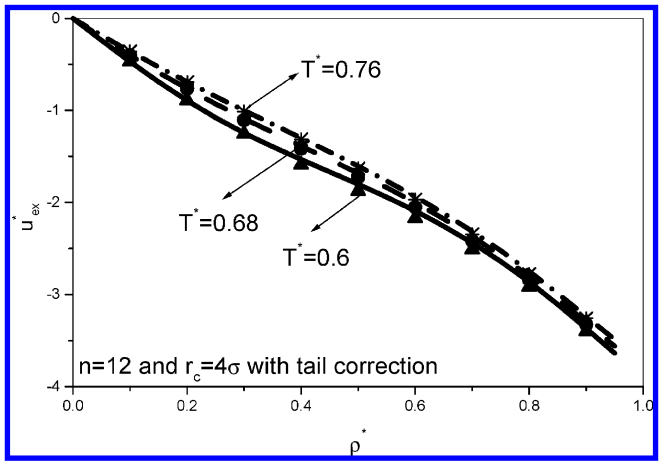

Figure 9. Same as in Figure 8, but the results are for the reduced excess internal energy u^*_{ex}.

practices of the OZ IET; the origin of such phenomena is based on the fact that each of all OZ closure approximations is actually equal to some kind of functional perturbation expansion approximation from the point of view of classical density

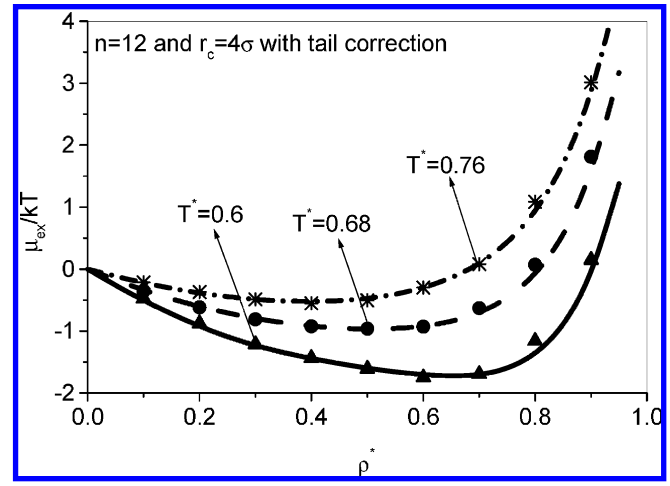

Figure 10. Same as in Figure 8, but the results are for the reduced excess chemical potential μ_{ex}/k_BT.

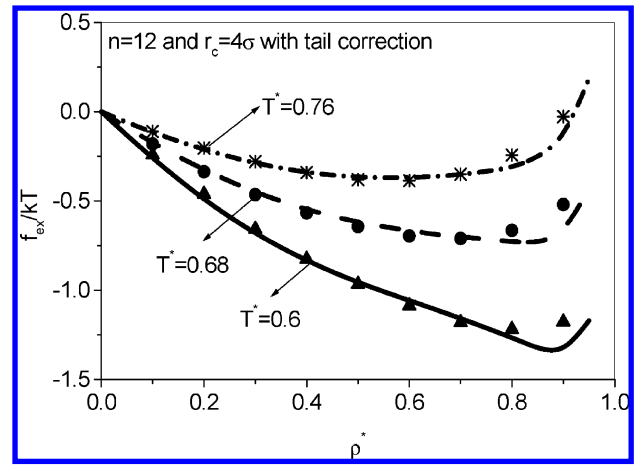

Figure 11. Same as in Figure 8, but the results are for the reduced excess free energy f_{ex}/k_BT.

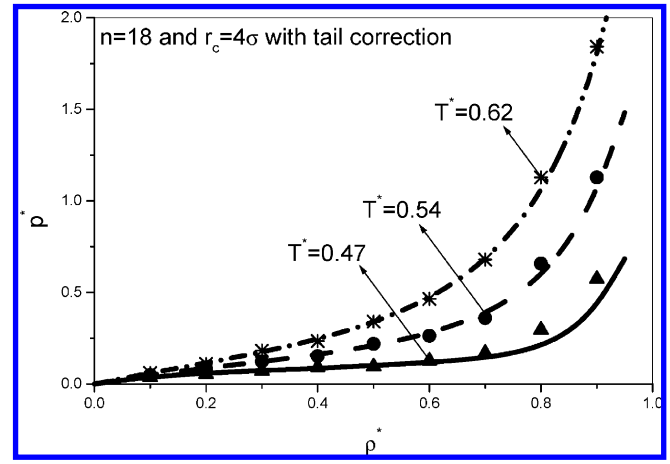

Figure 12. The reduced pressure p^* along with an isothermal line. The calculations are for the GLJ $2n - n$ fluid with $n = 18$ and several different temperature values as shown; the potential is truncated at $r_c = 4\sigma$ but not shifted, and the simulated pressures are corrected with tail contributions in a mean field approximation. Circles represent the present computer simulation data, whereas lines are for the present theoretical calculation results for the full potential.

functional theory (DFT); with shortening of the potential range, the temperature of interest decreases and the reduced perturbation part of the potential, i.e., the actual perturbation potential normalized by k_BT, increases; it is well-known that methods of perturbation category will become less successful when the

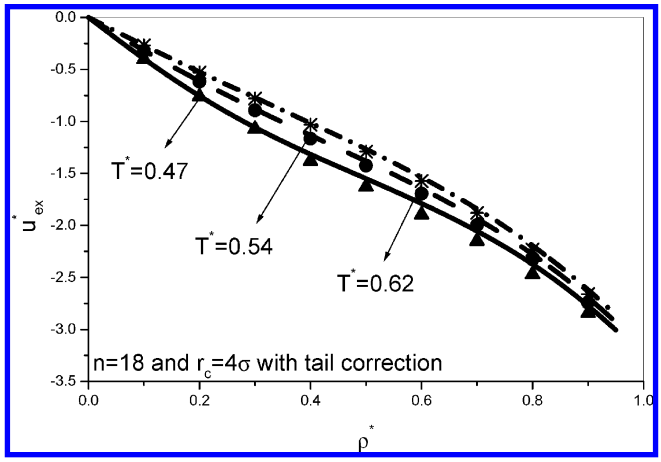

Figure 13. Same as in Figure 12, but the results are for the reduced excess internal energy u^*_{ex}.

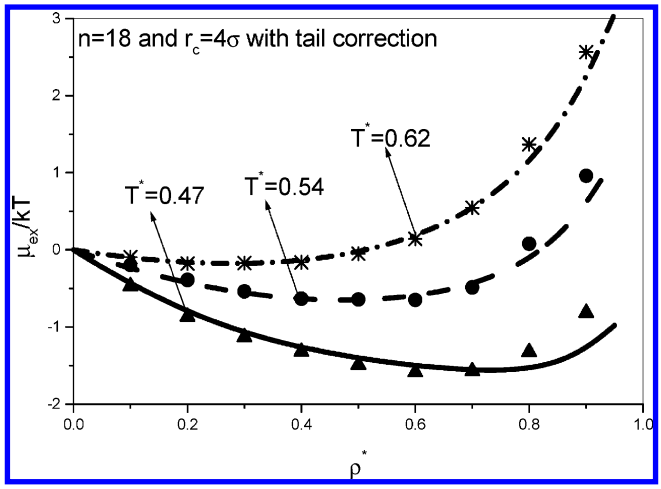

Figure 14. Same as in Figure 12, but the results are for the reduced excess chemical potential μ_{ex}/k_BT.

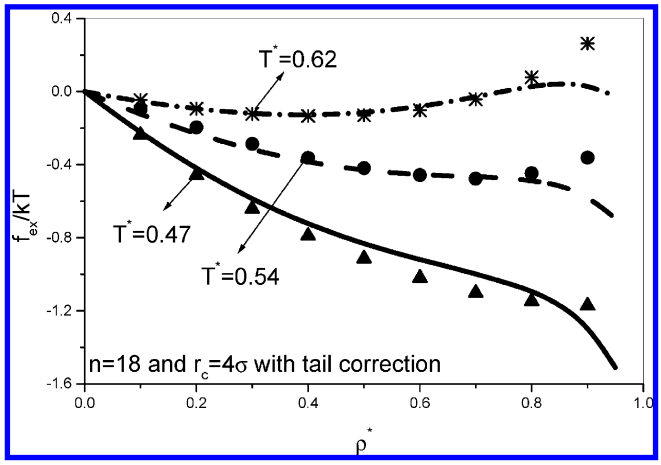

Figure 15. Same as in Figure 12, but the results are for the reduced excess free energy f_{ex}/k_BT.

strength of the perturbation term is much larger than one; this explains why all liquid state theories become more and more unsuccessful when the low temperature case is being dealt with. (ii) Along with getting deeper and deeper into the liquid−solid coexistence region, the present local self-consistent OZ IET becomes more and more insufficient; this phenomena can be clearly detected from the observation that the theoretical accuracy declines in the high density domain for the four thermodynamic quantities, and the performance deterioration is somewhat extraordinarily evident for the case of the excess free energy; particularly, the more short-ranged the potential and the lower the temperature, the smaller the threshold density beyond which the performance for the excess free energy begins to deteriorate obviously. As pointed out above, the performance deterioration in the solid−liquid coexistence region can be attributed to the formation of quasi-crystalline clusters and the fact that liquid state theories are incapable of a description of crystalline structures. As for the relation among the threshold density, potential range, and temperature, it obviously originates from the fact that the critical temperature decreases and the solid−liquid coexistence domain widens as the potential range becomes shorter; along with the decreasing of the temperature of interest and widening of the solid−liquid coexistence domain, the density of the liquid phase coexisting with the solid phase decreases and thus the threshold density also decreases. Although the performance deterioration is evident for the case of the excess free energy, it is not so obvious for the other three thermodynamic quantities; apparently, this is due to the double approximations involved with the theoretical calculation of the excess free energy. What truly reflects the quality of the closure approximation and the present local procedure for determining the value of d_e is the virial pressure and excess internal energy because of their direct connection with the structural functions as formulated in eqs 9 and 12; encouragingly, in spite of the demanding computed object, both the pressure and excess internal energy are dealt with efficaciously in the framework of the present local self-consistent OZ IET. Once the structural functions are proved to be fully correct, the quality of the local expression in eq 13 is trustily measured by the accuracy of the excess chemical potential predicted by eq 13; what emerges from Figures 8−15 is a self-consistent picture: the accuracy of predicted excess chemical potential changes synchronously with that of both the pressure and excess internal energy; this is exactly a representation of the validity of the local expression in eq 13.

IV. Conclusion

To end the presentation, several concluding remarks are drawn from the results and discussions presented.

(i) For the GLJ $2n - n$ fluid with potential exponent n ranging from long-ranged to short-ranged to very short-ranged, the local self-consistent OZ IET generally behaves well for two structural properties, namely, rdf and static structure factor, and two thermodynamic properties, namely, pressure and excess internal energy. These four quantities are direct outcomes of the OZ IET, and there is no need for any approximations to obtain them once the OZ IET is completely defined; consequently, satisfactory predictions of these four properties trustily reflect the effectiveness of both the closure approximation and local procedure for determining the value of the adjustable parameter d_e. Since the effectiveness persists to very low temperature and very short-ranged potential, certainly there is a deeper reason for this abnormal success, and there is a necessity to explore the reason in future research.

(ii) The local formulation for calculation of the excess chemical potential is itself valid; as long as the structural functions are dependable, the calculated excess chemical potential is also trustworthy. It is noted that the calculation of the excess chemical potential is mainly affected by the contribution of $B(r)$ inside the core (98% in the case of the hard sphere fluid[17]), and this explains the necessity that we supplement the ML hard sphere bridge function by the simulation-fitting GvEF−BS−VW hard sphere bridge function for $r < \sigma_{HS}$, since

the ML hard sphere bridge function is only after rigorous testing for the $r > \sigma_{HS}$ domain, its validity for the $r < \sigma_{HS}$ domain is never tested.[18] In fact, the ML hard sphere bridge function for $r < \sigma_{HS}$ is even qualitatively improper compared to the simulation-fitting GvEF−BS−VW hard sphere bridge function for $r < \sigma_{HS}$. Encouragingly, using the same structural functions from the present local self-consistent OZ IET, the previously derived local expression denoted by eq 13 has by and large the same accuracy in calculating for the excess chemical potential as the exact virial pressure formula for the pressure.

(iii) In the low temperature and high density domain, the present local self-consistent OZ IET exhibits some deviations from the "exact" simulation results, which, we think, originates from the formation of quasi-crystalline clusters; this only reflects that the description of crystalline structures goes beyond the current OZ IET framework; the deviation becomes a little serious for the excess free energy, and this is additionally attributed to double approximations involved to obtain the excess free energy from the structural functions. As a result, it seems necessary to devise a new local formulation capable of calculation of the excess free energy directly from the structural functions of the state point of interest; we will report such a local expression in the near future.

(iv) It would be advisible to give a comparison between the present local self-consistent OZ IET and other more traditional methods. First, we will compare the present approach with the traditional thermodynamic perturbation theory (TPT). The traditional TPT approaches are mostly truncated at first order or second order by discarding the contributions stemming from the higher-order terms, and the truncation is in fact unavoidable because of lack of methods appropriate for calculating higher-order correlation functions indispensable in calculating the higher-order terms. Along with a decrease of the temperature of interest, the strength of the perturbation part will tend to increase; the concomitancy is that the contributions from the ignored higher-order terms will exceed those stemming from the retained terms. Consequently, the TPT will become less and less satisfactory along with the investigated temperature entering into the low temperature domain of current interest. From the point of view of density functional theory, the usual HNC approximation for the bridge function, i.e., $B(r) = 0$, corresponds to a second-order functional perturbation expansion, and therefore, the bridge function $B(r)$ encompasses all contributions stemming from higher-order terms beyond second-order truncation. Any qualified approximation for $B(r)$ necessarily adequately accounts for all of the discarded terms as a whole beyond the second-order term, and this is in contrast with the TPT which separately attacks each of the retained terms. As a result, in the case of low temperature, performance deterioration of the OZ IET is far less acute than the traditional TPT. An advantage of the TPT is that it directly calculates the excess Helmholtz free energy, and then all of the other thermodynamic quantities can be obtainable directly. In traditional OZ IET, the thermodynamic integration along an isothermal path or the Kirkwood charging process[15] are involved to calculate the excess chemical potential, and then the excess Helmholtz free energy, and this undoubtedly incurs an enormous computational load. Inspiringly, the local formulation in eq 13 enables the straightforward calculation of these two quantities in the framework of the OZ IET, and the combination of "local properties" in both specifying the effective hard sphere diameter d_{eff} and determining the excess chemical potential truly makes the OZ IET approach the same effective in computing the energy properties as the TPT approach.

Acknowledgment. This project is supported by the National Natural Science Foundation of China (No. 20973202).

Appendix

The hard sphere bridge function B_{HS}, proposed in ref 13, is a hybrid of an earlier empirical hard sphere bridge function B_{ML} and a recently proposed simulation data-fitting hard sphere bridge function $B_{GvEF-BS-VW}$. Details of B_{ML} can be found in ref 14, whereas the details of the ingredients comprised of $B_{GvEF-BS-VW}$ are not reported in the original paper.[12] Now we will report the mathematical details of $B_{GvEF-BS-VW}$. Reference 12 proposes a hard sphere bridge function approximation given as

$$B_{GvEF-BS-VW}(r) = \begin{cases} \ln(y_{HS}(r)) + 1 + C^{(2)}_{0HS}(r) & r < \sigma_{HS} \\ \ln(g_{HS}(r)) + C^{(2)}_{0HS}(r) + 1 - g_{HS}(r) & r > \sigma_{HS} \end{cases} \quad \text{(A1)}$$

Individual terms in eq A1 are given by semitheoretical simulation data-fitting formulas of different authors, i.e., of Groot, van der Erden, and Faber,[19] Balance and Speedy,[20] and Verlet and Weis.[21] This function is therefore denoted as the GvEF−BS−VW hard sphere bridge function, as suggested in the work of ref 12 by the present author.

Reference 20 gave a simple expression for $\ln(y_{HS}(r))$, the logarithm of the hard sphere cavity correlation function

$$\ln(y_{HS}(r)) = \ln(y_{HS}(0)) + \Delta V(r)(a_1 + a_2 r) \quad \text{(A2)}$$

Here, $\ln(y_{HS}(0)) = \beta\mu_{exHS}$, and the excess chemical potential μ_{exHS} for the hard sphere fluid is given by a simple expression stemming from a Carnhan−Starling (CS) equation of state (EoS)[22]

$$\beta\mu_{exHS} = (8\eta - 9\eta^2 + 3\eta^3)/(1 - \eta)^3 \quad \text{(A3)}$$

where $\eta = \rho_{HS}\sigma_{HS}^3\pi/6$ is the hard sphere packing fraction, ρ_{HS} and σ_{HS} are, respectively, the hard sphere number density and diameter as remarked previously in the text. $\Delta V(r)$ is calculated by the following expression

$$\Delta V(r) = (2\pi/3)\sigma_{HS}^3(3x - x^3) \quad \text{(A4)}$$

where $x = r/(2\sigma_{HS})$; a_1 and a_2 are determined by eqs A5 and A6

$$a_1 = -\rho_{HS} g_{HS}(\sigma_{HS}) \quad \text{(A5)}$$

$$a_2 = (\ln\{\exp(-\beta\mu_{exHS}) g_{HS}(\sigma_{HS})\}/\Delta V(\sigma) - a_1)/\sigma_{HS} \quad \text{(A6)}$$

where $g_{HS}(\sigma_{HS})$, the value of hard sphere rdf $g_{HS}(r)$ at $r = \sigma_{HS}$, is also specified by the CS EoS, and is given by

$$g_{HS}(\sigma_{HS}) = (1 - \eta/2)/(1 - \eta)^3 \quad \text{(A7)}$$

$C^{(2)}_{0HS}(r)$, the second order DCF of the hard sphere fluid, is given by the simulation data-fitting formula proposed in ref 19

$$C^{(2)}_{0HS}(r) = \begin{cases} c_0 + c_1 r^* + c_2 r^{*2} + c_3 r^{*6} & r^* < 1 \\ r^{*-2}[d_1(2 - r^*)^6 + d_2(2 - r^*)^9 + d_3 \sin(4\pi r^*)] & 1 < r^* < 2 \\ 0 & r^* > 2 \end{cases} \quad \text{(A8)}$$

where $r^* = r/\sigma_{HS}$, and the coefficients d_m are given by

$$d_1 = -[0.1\eta^2 + (4/3)\eta^3]/(1 - \eta)^4 \quad \text{(A9)}$$

$$d_2 = 1.1\eta^2/(1 - \eta)^4 \quad \text{(A10)}$$

$$d_3 = -[(1/15)\eta^3]/(1 - \eta)^4 \quad \text{(A11)}$$

The c_m's are functions of the density, and are given by

$$c_m(\eta) = \sum_{n=0}^{3} W_{mn}\eta^n/(1 - \eta)^4 \quad \text{(A12)}$$

where the W matrix is given by eq 31 in ref 19 and is not repeated here; interested readers can refer to ref 19 for details. Finally, the hard sphere rdf $g_{HS}(r)$ is given by a semitheoretical simulation data-fitting VW expression,[21] which is lengthy and not repeated here; interested readers can refer to ref 21 for details.

It is noted that the three semitheoretical expressions[19−21] for $\ln(y_{HS}(r))$, $C^{(2)}_{0HS}(r)$, and $g_{HS}(r)$ are consistent with the CS EoS;[22] the resultant $B_{GvEF-BS-VW}(r)$ is, as expectedly, continuous at $r = \sigma_{HS}$. However, combination of the three expressions of different origins may generate a tiny error; consequently, the hybrid hard sphere bridge function B_{HS} employs B_{ML} of single source for the $r > \sigma_{HS}$ domain, since B_{ML} is put through the test for this domain. It is noted[18] that for the $r < \sigma_{HS}$ domain the B_{ML} hard sphere bridge function exhibits behavior qualitatively different from $B_{GvEF-BS-VW}(r)$; therefore, the hybrid hard sphere bridge function B_{HS} uses $B_{GvEF-BS-VW}(r)$ for the $r < \sigma_{HS}$ domain. As for the constant "Cons", its existence is to guarantee the continuity of B_{HS} at $r = \sigma_{HS}$.

References and Notes

(1) Hill, T. L. *Introduction to statistical thermodynamics*; Addison Wesley: New York, 1960. Martynov, G. A. *Phys. Rev. E* **2009**, *79*, 031119.

(2) Mitchell, D. J.; Ninham, B. W. *J. Chem. Phys.* **1972**, *56*, 1117. Nobre, T. M.; Silva, H. D. E.; Furriel, R. P. M.; Leone, F. A.; Miranda, P. B.; Zaniquelli, M. E. D. *J. Phys. Chem. B* **2009**, *113*, 7491. Ionita, G.; Florent, M.; Goldfarb, D.; Chechik, V. *J. Phys. Chem. B* **2009**, *113*, 5781. Wheatley, R. J.; Harvey, A. H. *J. Chem. Phys.* **2009**, *131*, 154305. Perez-Lopez, S.; Vila-Romeu, N.; Esteller, M. A. A.; Espina, M.; Haro, I.; Mestres, C. *J. Phys. Chem. B* **2009**, *113*, 319.

(3) Khanpour, M.; Hashim, R. *J. Chem. Phys.* **2008**, *129*, 164508. Ben-Naim, A. *J. Chem. Phys.* **2008**, *129*, 104506. Liu, B.-T.; Hsu, J.-P. *J. Chem. Phys.* **2009**, *130*, 044106. dell'Erba, M. G.; Zemba, G. R. *Phys. Rev. E* **2009**, *79*, 011913.

(4) Lee, S.-W.; Sigmund, W. M. *J. Colloid Interface Sci.* **2001**, *243*, 365.

(5) (a) Roth, C. M.; Neal, B. L.; Lenhoff, A. M. *Biophys. J.* **1996**, *70*, 977. (b) Vaitheeswaran, b. S.; Reddy, G.; Thirumalai, D. *J. Chem. Phys.* **2009**, *130*, 094502. (c) Izevkov, S.; Swanson, J. M. J.; Voth, G. A. *J. Phys. Chem. B* **2008**, *112*, 4711. (d) Harano, Y.; Yoshidome, T.; Kinoshita, M. *J. Chem. Phys.* **2008**, *129*, 145103. (e) Saija, F.; Prestipino, S.; Malescio, G. *Phys. Rev. E* **2009**, *80*, 031502. (f) Grandner, S.; Zeng, Y.; Klitzing, R. v.; Klapp, S. H. L. *J. Chem. Phys.* **2009**, *131*, 154702. (g) Verwey, E. J. W.; Overbeek, J. T. G. *Theory of Stability of Lyophobic Colloids*; Elsevier: Amsterdam, The Netherlands, 1948.

(6) Hasegawa, M.; Ohno, K. *J. Phys.: Condens. Matter* **1997**, *9*, 3361.

(7) Vliegenthart, G. A.; Lodge, J. F. M.; Lekkerkerker, H. N. W. *Physica A* **1999**, *263*, 378.

(8) (a) Hansen, J. P.; McDonald, I. R. *Theory of simple liquids*, 2nd ed.; Academic Press: London, 1986. (b) Quesada-Perez, M.; Callejas-Fernandez, J.; Hidalgo-Alvarez, R. *Colloids Surf., A* **1999**, *159*, 239. (c) Quesada-Perez, M.; Gonzalez-Tovar, E.; Martin-Molina, A. *Colloids Surf., A* **2005**, *267*, 24. (d) Jagannathan, K.; Reddy, G.; Yethiraj, A. *J. Phys. Chem. B* **2005**, *109*, 6764. (e) Duda, Y.; Ochoa, F. L.; Trokhymchuk, A. *Colloids Surf., A* **2000**, *161*, 477. (f) Deniz, V.; Bostrom, M.; Bratko, D. *Colloids Surf., A* **2008**, *319*, 98.

(9) Lee, L. L. *Molecular Thermodynamics of Nonideal Fluids*; Butterworth Publishers: 1988.

(10) Rogers, F. J.; Young, D. A. *Phys. Rev. A* **1984**, *30*, 999. Zerah, G.; Hansen, J. P. *J. Chem. Phys.* **1985**, *84*, 2336. Lee, L. L. *J. Chem. Phys.* **1995**, *103*, 9388. Chung, T. H.; Lee, L. L. *J. Chem. Phys.* **2009**, *130*, 134513.

(11) Caccamo, C.; Pellicane, G. *J. Chem. Phys.* **2002**, *117*, 5072. Borge, A.; Høye, J. S. *J. Chem. Phys.* **1998**, *108*, 4516. Bomont, J. M.; Bretonnet, J. L. *J. Chem. Phys.* **2001**, *114*, 4141.

(12) Zhou, S. *Theor. Chim. Acta* **2007**, *117*, 555.

(13) Zhou, S. *Phys. Rev. E* **2009**, *79*, 011126.

(14) Malijevsky, A.; Labik, S. *Mol. Phys.* **1987**, *60*, 663.

(15) Kirkwood, J. G. *J. Chem. Phys.* **1935**, *3*, 300.

(16) Frenkel, D.; Smit, B. *Understanding Molecular Simulation*; Academic: Boston, MA, 1996.

(17) Lee, L. L. *J. Chem. Phys.* **1992**, *97*, 8606.

(18) Zhou, S. *Chem. Phys.* **2006**, *330*, 478.

(19) Groot, R. D.; van der Eerden, J. P.; Faber, N. M. *J. Chem. Phys.* **1987**, *87*, 2263.

(20) Ballance, J. A.; Speedy, R. J. *Mol. Phys.* **1985**, *54*, 1035.

(21) Verlet, L.; Weis, J.-J. *Phys. Rev. A* **1972**, *5*, 939.

(22) Carnhan, N. F.; Starling, K. E. *J. Chem. Phys.* **1969**, *51*, 635.

JP1038317